Title

Efficient and facile delivery of gold nanoparticles in vivo using dissolvable microneedles for contrast-enhanced optical coherence tomography

Journal

Biomedical Optics Express, 1(1)

ISSN

2156-7085

Authors

Kim, Chang Soo
Ahn, Yeh-Chan
Wilder-Smith, Petra
et al.

Publication Date

2010-07-14

Efficient and facile delivery of gold nanoparticles *in vivo* using dissolvable microneedles for contrast-enhanced optical coherence tomography

Chang Soo Kim,[1,2] Yeh-Chan Ahn,[3] Petra Wilder-Smith,[2] Seajin Oh,[4] Zhongping Chen,[1,2,5,7] and Young Jik Kwon[1,5,6,8]

[1]*Department of Chemical Engineering and Materials Science, University of California, Irvine, Irvine, CA 92697, USA*
[2]*Beckman Laser Institute, University of California, Irvine, Irvine, CA 92612, USA*
[3]*Department of Biomedical Engineering, Pukyong National University, Busan 608-737, Korea*
[4]*TheraJect, Inc., Fremont, CA 94538, USA*
[5]*Department of Biomedical Engineering, University of California, Irvine, Irvine, CA 92697, USA*
[6]*Department of Pharmaceutical Sciences, University of California, Irvine, Irvine, CA 92697, USA*
[7]*z2chen@uci.edu*
[8]*kwonyj@uci.edu*

Abstract: Obtaining sufficient contrast is an indispensable requirement for detecting early stage cancer using optical coherence tomography (OCT), an emerging diagnostic tool that detects abnormal lesions with micrometer resolutions in real time. PEGylated gold nanoparticles (Au NPs; 87 nm in diameter) were formulated in aqueous dissolvable microneedles (dMNs; 200 μm height) for efficient, precisely controlled, and convenient delivery of Au NPs into hamster oral tissue *in vivo*. The Au NPs were then further briefly dissipated by ultrasound (US). The results showed 33% and 20% increase in average optical scattering intensity (contrast level) in dysplastic and normal tissues, respectively, and pinpointed pathological structures of early stage oral cancer were also identified by the highly convenient and efficient administration of Au NPs in a novel delivery platform.

OCIS codes: (160.4236) Nanomaterials; (110.4500) Optical coherence tomography.

References and links

1. D. Huang, E. A. Swanson, C. P. Lin, J. S. Schuman, W. G. Stinson, W. Chang, M. R. Hee, T. Flotte, K. Gregory, C. A. Puliafito, and J. G. Fujimoto, "Optical coherence tomography," Science **254**(5035), 1178–1181 (1991).
2. J. G. Fujimoto, M. E. Brezinski, G. J. Tearney, S. A. Boppart, B. Bouma, M. R. Hee, J. F. Southern, and E. A. Swanson, "Optical biopsy and imaging using optical coherence tomography," Nat. Med. **1**(9), 970–972 (1995).
3. M. E. Brezinski, G. J. Tearney, B. E. Bouma, J. A. Izatt, M. R. Hee, E. A. Swanson, J. F. Southern, and J. G. Fujimoto, "Optical coherence tomography for optical biopsy. Properties and demonstration of vascular pathology," Circulation **93**(6), 1206–1213 (1996).
4. A. Sergeev, V. Gelikonov, G. Gelikonov, F. Feldchtein, R. Kuranov, N. Gladkova, N. Shakhova, L. Snopova, A. Shakhov, I. Kuznetzova, A. Denisenko, V. Pochinko, Y. Chumakov, and O. Streltzova, "In vivo endoscopic OCT imaging of precancer and cancer states of human mucosa," Opt. Express **1**(13), 432–440 (1997).
5. T. Ohira, Y. Suga, Y. Nagatsuka, J. Usuda, M. Tsuboi, T. Hirano, N. Ikeda, and H. Kato, "Early-stage lung cancer: diagnosis and treatment," Int. J. Clin. Oncol. **11**(1), 9–12 (2006).
6. C. S. Kim, P. Wilder-Smith, Y. C. Ahn, L. H. Liaw, Z. Chen, and Y. J. Kwon, "Enhanced detection of early-stage oral cancer in vivo by optical coherence tomography using multimodal delivery of gold nanoparticles," J. Biomed. Opt. **14**(3), 034008 (2009).
7. M. J. Yadlowsky, J. M. Schmitt, and R. F. Bonner, "Multiple scattering in optical coherence microscopy," Appl. Opt. **34**(25), 5699–5707 (1995).
8. Y. T. Pan, R. Birngruber, and R. Engelhardt, "Contrast limits of coherence-gated imaging in scattering media," Appl. Opt. **36**(13), 2979–2983 (1997).
9. U. Sharma, E. W. Chang, and S. H. Yun, "Long-wavelength optical coherence tomography at 1.7 microm for enhanced imaging depth," Opt. Express **16**(24), 19712–19723 (2008).
10. S. A. Boppart, A. L. Oldenburg, C. Xu, and D. L. Marks, "Optical probes and techniques for molecular contrast enhancement in coherence imaging," J. Biomed. Opt. **10**(4), 041208 (2005).

#130172 - $15.00 USD Received 15 Jun 2010; accepted 7 Jul 2010; published 14 Jul 2010

11. V. P. Zharov, J. W. Kim, D. T. Curiel, and M. Everts, "Self-assembling nanoclusters in living systems: application for integrated photothermal nanodiagnostics and nanotherapy," Nanomedicine **1**(4), 326–345 (2005).
12. G. Frens, "Controlled nucleation for the regulation of the particle size in monodisperse gold suspensions," Nat. Phys. Sci (Lond.) **241**, 20–22 (1973).
13. W. Haiss, N. T. Thanh, J. Aveyard, and D. G. Fernig, "Determination of size and concentration of gold nanoparticles from UV-vis spectra," Anal. Chem. **79**(11), 4215–4221 (2007).
14. J. Aaron, N. Nitin, K. Travis, S. Kumar, T. Collier, S. Y. Park, M. José-Yacamán, L. Coghlan, M. Follen, R. Richards-Kortum, and K. Sokolov, "Plasmon resonance coupling of metal nanoparticles for molecular imaging of carcinogenesis in vivo," J. Biomed. Opt. **12**(3), 034007 (2007).

1. Introduction

Optical coherence tomography (OCT) is a non-invasive (or minimally invasive) optical imaging tool that detects scattering signals from tissues irradiated with near-infrared (NIR) laser light [1]. OCT is capable of a real time "optical biopsy", visualizing the morphology of a target tissue with micrometer resolution in real time [2,3], with many important potential applications, such as diagnosing early stage carcinoma within the OCT's imaging depth of a few mm [4,5]. However, the use of high-resolution OCT for diagnosis of early stage cancer is still limited because of the difficulty in obtaining sufficiently high optical contrast in deep tissue by overcoming multiple photon scattering [6–9]. Various NIR dyes (e.g., indocyanine green, ICG) and micro- and nanoparticles have been explored as OCT contrast agents [10]. Despite the great interest in employing gold nanoparticles (Au NPs) by using their high biocompatibility and superior optical properties, efficient delivery of Au NPs to specific target tissues has been a major hurdle [10,11]. Recently, we reported significantly enhanced OCT imaging of early stage oral cancer via a multimodal Au NP delivery method by combining tissue penetration by Au NPs using microneedles (MNs) with Au NP dissipation using ultrasound (US) [6]. However, topical delivery of an Au NP-containing solution onto microchannels produced by the use of a stainless steel MN roller is not an ideal mode of administration. First, a majority of Au NPs simply remain deposited on the outer tissue surface (e.g., stratum corneum, SC) instead of being delivered through the MN-created passages (poor efficiency). Second, it is almost impossible to predict/quantify the amount of Au NPs delivered into the tissue (unrepeatable dose control). Finally, the use of a stainless steel MN roller followed by topical application of Au NP-containing solution on the MN-applied area, then wiping deposited Au NPs into the tissue surface, is inconvenient and imprecise.

In this study, Au NPs were formulated into dissolvable microneedles (dMNs) in order to overcome the limitations mentioned above. Au NPs (87 nm in diameter) were mixed in sodium carboxymethyl cellulose (SCMC) solution. Then the mixture was cast into an array of needle-shaped holes by centrifugation and air-dried in order to obtain Au NP-containing dMNs. Advantages of this approach include: (1) Au NPs are concentrated at the tips of dMNs to maximize NP delivery into target tissue; (2) Penetration depth of Au NPs (locations of Au NPs) can be easily controlled by the length of dMNs,(3) Au NPs can be conveniently administered simply by applying dMNs (no separate steps of MN application, dropping Au NP-containing solution, and wiping surface-deposited Au NPs); (4) dMNs are biocompatible and do not need to be removed after use.

The hamster cheek pouch carcinogenesis model was used to generate oral dysplasia in order to investigate *in vivo* contrast-enhanced OCT imaging using Au NP-containing dMNs. Using a spectral domain OCT (SD-OCT) system, significantly increased average scattering signals were confirmed in dysplastic and normal tissues using the proposed approach, and more importantly, abnormal structures in dysplastic tissues were clearly distinguished by OCT. Therefore, dMNs provide a promising and novel device platform for contrast-enhanced OCT imaging via multimodal administration of Au NPs.

#130172 - $15.00 USD Received 15 Jun 2010; accepted 7 Jul 2010; published 14 Jul 2010

2. Methods

2.1 Synthesis of Au NPs

Scattering dominant, citrate capped Au NPs (70 nm in diameter) were synthesized by Frens' method [12] with a slight modification as reported previously [6]. The size of resulting Au NPs was measured by using dynamic light scattering (DLS) particle analysis using a Melvern Zetasizer as well as transmission electron microscopy (TEM). The final Au NP concentration was determined to be 6.94×10^9 particles/mL by UV/vis spectroscopy [13]. The surface of Au NPs were PEGylated by activating the surface with *N* -succinimidyl 3-(2-pyridyldithio)-propionate (SPDP) and reacting with amine-activated polyethylene glycol (PEG; 2 kDa). Briefly, Au NPs were washed with DI water by centrifugation at 4,600 rpm for 10 min three times. Sixty mL of Au NPs were gradually added to vigorously stirred 12 μL of 20 mM SPDP on ice using a peristatic pump at 7 μL/s flow rate. The mixture remained stirred in room temperature overnight. After unreacted SPDP was removed by centrifugation at 4,600 rpm for 10 min three times, 60 mL of SPDP-activated Au NPs were added to 45.6 μL of amine-PEG (10 mg/mL) with vigorous stirring, followed by incubation at room temperature overnight. Unreacted amine-PEG was removed by centrifugation three times at 4,600 rpm for 30 min. The size of the PEGylated Au NPs was determined to be 87 nm in diameter by DLS at the final concentration of 6.41×10^8 particles/mL.

2.2 Fabrication of Au NP-containing dissolvable microneedles

Briefly, a metal pyramid-shape MN array was fabricated by precision machining to obtain a sharp tip apex of 10-20 μm radius. The length of the pyramid needles was 200 μm with the height to base ratio of 2.3. The density of needles in the area was 400/cm^2. A silicone mold was cast from the metal needle array and used to produce dissolvable Au NP MNs. Sodium carboxylmethyl cellulose (SCMC, 90kDa) (Sigma, St. Louis, MO) that is relatively highly aqueous soluble and mechanically robust in a dry form was mixed with sucrose (Hercules Inc., Wilmington, DE) at a 1:3.75 weight ratio (SCMC:sucrose) to accelerate dissolution in tissue. Au NP-containing solution (200 μL, Au NP concentration: 1.92×10^{10} particles/mL) was mixed with the SCMC-sucrose solution (100 μL of 8% SCMC and 30% sucrose). To fabricate the Au NP-concentrated tip needles, the Au NP-containing SCMC-sucrose solution was spun on the mold at 4,000 rpm for 5 minutes to fill the needle-shaped cavities and concentrate Au NPs at the cavity end, immediately followed by removal of residual excess from the exterior of the needle-shaped cavities. In the second coating, the Au NP-free solution was added onto the mold to form a MN-immobilizing disc layer. After air-drying for 24 h, Au NP-containing dMNs on a 1 cm disc were obtained (Fig. 1). When the SCMC-sucrose solution was dried in the mold, its volume shrank by 80% towards the cavity end, thus retaining Au NP at the end of the microneedle structures.

Fig. 1. Au NP-containing dissolvable microneedles (dMNs) arrayed on a dissolvable disc (1 cm in diameter).

2.3 In vivo hamster oral cancer model and histology

Golden Syrian hamsters (*Mesocricetus auratus*) were topically treated with 0.5% (w/v) 9, 10-dimethyl-1,2-benzanthracene (DMBA, Sigma) in mineral oil three times per week for 10 wks to induce dysplasia in one cheek pouch in each animal (in accordance with UCI IACUC protocol approval 97-1972). The other contralateral cheek pouch remained untreated. Imaging

#130172 - $15.00 USD Received 15 Jun 2010; accepted 7 Jul 2010; published 14 Jul 2010

was performed in the cheek pouch of the anesthetized hamster by gently clamping the tissues to a microscope stage using a custom-built, ring-shaped clamp (Fig. 2). The ring was used to ensure accurate co-localization of subsequent imaging episodes. After Au NP administration by combined dMN and US, DMBA-treated and untreated hamster cheek pouch tissues were harvested and fixed for a day in 10% formalin buffer followed by transfer to phosphate buffered saline (PBS) solution. The paraffin-embedded tissues were sectioned at 6 μm thickness for a hematoxylin and eosin (H&E) staining. The stained tissues were visualized under a microscope equipped with an Olympus Microfire digital camera (Olympus, Tokyo, Japan).

Fig. 2. DMBA-treated hamster cheek pouch attached to a microscope stage using a custom-built, ring-shaped clamp (1 cm in diameter).

2.4 OCT imaging and signal quantification

A SD-OCT system (Fig. 3) was used to obtain OCT images from the hamster cheek pouch tissues. Specifications of the SD-OCT system include low-coherence light with 1310 nm of center wavelength and 90 nm of full width at half maximum (FWHM), a 1 × 1024 InGaAs detector array at 7.7 kHz frame rate with a 130 nm wide spectrum, and a 2-axis scanner with two galvanometers located at the same sample arm. Imaging depth and depth resolution were 3.4 mm and 8 μm in air, respectively, and SD-OCT images were obtained at the same focal point throughout the study.

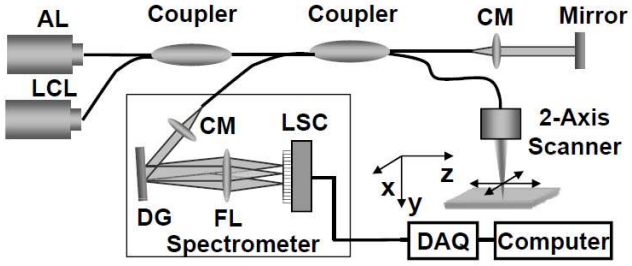

Fig. 3. Schematic of optical fiber-based spectral-domain (SD)-OCT system: AL, aiming laser; CM, collimator; DAQ, data acquisition system; DG, diffraction grating; FL, focusing lens; LCL, low-coherence light; LSC, line scan camera.

Hamster cheek pouches were imaged before and after dMNs were administered and US was applied. Briefly, dMNs placed in the clamp's circular hole were pressed with a finger for 10 min. After applying US gel, a diagnostic level US force (1 MHz at 0.3 W/cm^2 power density) was applied using a Dynatron 125 ultrasonicator (Dynatronics Corporation, Salt Lake City, UT) for 1 min. The tissues were imaged using a SD-OCT at various time points up to 30 min. The area of interest (210 pixels long × 5 pixels wide) in the acquired OCT images was analyzed for OCT signal intensity using Scion image processing software, and the signals in three different areas were averaged for statistical significance.

#130172 - $15.00 USD Received 15 Jun 2010; accepted 7 Jul 2010; published 14 Jul 2010

3. Result and discussion

A major hurdle to the topical delivery of Au NPs is the stratum corneum (10-40 µm). The optimal penetration depth for diagnostic OCT imaging in the epithelial layer is in the range of 50-400 µm. Microscopy confirmed that Au NP-containing dMNs (Fig. 4a) had a height of 200 µm and ~85 µm base in a semi-transparent, sharp pyramid shape. Most noticeably, Au NPs had indeed been highly concentrated by centrifugation, forming a dark tip on each MN (Fig. 4a). The OCT image in Fig. 4b shows that a dMN was able to penetrate into the hamster cheek pouch tissue. The concave injection site caused by the dMN-pressing force indicates that Au NPs can be delivered at a depth of 100-200 µm, which meets the required penetration depth.

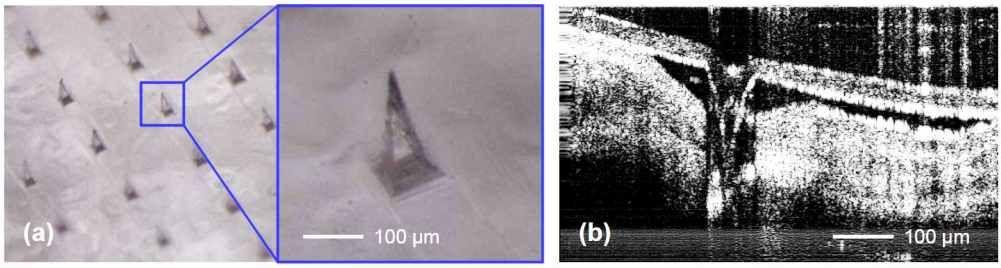

Fig. 4. Au NPs containing dissolvable microneedles (200 µm height).

OCT signals (scattering intensity) from normal and dysplastic tissues, before and after dMN application with US, were quantified (Fig. 5). The average OCT signal intensity from normal base tissue (i.e., without dMN and US application) was higher than that from dysplastic tissue, possibly because the process of carcinogenesis using the hamster cheek pouch model causes localized areas of epithelial thickening and increased keratinization which inhibit light penetration. Interestingly, however, once the dMN and US were applied, the intensity of the OCT signal increased by 33% in dysplastic tissue while only a 20% increase in OCT signal intensity was observed in normal tissues. It has been reported that as dysplasia develops and progresses, the epithelium loses its functions as a biological barrier, permitting increased penetration of contrast agents (i.e., PEGylated Au NPs) into the tissues [14]. Therefore, the higher OCT signal increase after dMN and US application observed in dysplastic tissue (Fig. 5) might be attributed to the presence in the tissues of a high number of Au NPs as well as an enhanced surface plasmon resonance (SPR) effect from co-localized Au NPs due to their high density in dysplastic tissue.

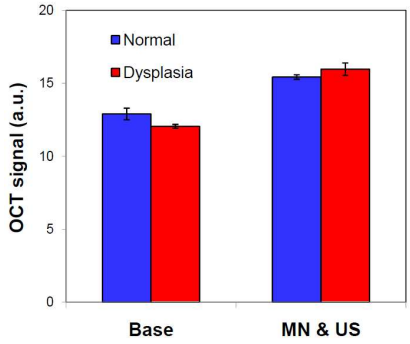

Fig. 5. Average SD-OCT signal (scattering intensity) from normal and dysplastic hamster oral tissues before and after dMN and US application.

The pathological characteristics of dysplasia were further observed by OCT (Fig. 6) and quantitatively compared (Fig. 7). Structural differences between dysplastic vs. normal tissue

#130172 - $15.00 USD Received 15 Jun 2010; accepted 7 Jul 2010; published 14 Jul 2010

were evident after the application of dMNs and US. Disrupted vs. well-aligned epithelial stratification was apparent as shown in Figs. 6c and 6d, respectively. Overall, optical contrast levels in the epithelial layer (green areas in Fig. 7) increased in dysplastic and normal tissues after dMNs and US had been applied. Analysis of quantitative depth-dependent distributions of OCT signal intensity (Fig. 7) indicates a couple of key differences between dysplastic and normal tissues, before and after dMN and US had been applied. First, the OCT signal intensity in the stratum corneum (SC, yellow areas in Fig. 7) increased in dysplastic tissue after dMNs and US had been applied (Fig. 7a) whereas signals did not change markedly in normal tissue (Fig. 7b). This is consistent with a previous finding that more Au NPs were accumulated in the SC of dysplastic tissue than normal tissue [6]. Second and most importantly, the signal intensity profiles in the normal epithelial layer before and after dMNs and US had been applied were fairly well-matched. In contrast, a dramatic optical contrast (blue area in Fig. 7) ensued in the dysplastic epithelial layer after dMNs and US had been applied. For comparison, a very similar level of OCT signals was obtained in the dysplastic epithelial layer, regardless of depth, before dMNs and US had been applied (blue line in Fig. 7a). The results shown in Figs. 6 and 7 demonstrate that clear and quantitative imaging-based differences between dysplastic and normal tissues were obtained by administering Au NPs in dMNs in combination with a brief and mild US stimulation. It should be emphasized that the amount of Au NPs formulated in the dMNs used in this study was approximately 200 times less than what was used in a previous study utilizing stainless steel MNs pre-treatment, topical application of Au NP-containing solutions, wiping of surface-deposited Au NPs, and US application. Therefore, dMNs are a highly convenient, precisely dose-controllable, and an efficient platform to deliver Au NPs for contrast-enhanced detection of early stage cancer using OCT.

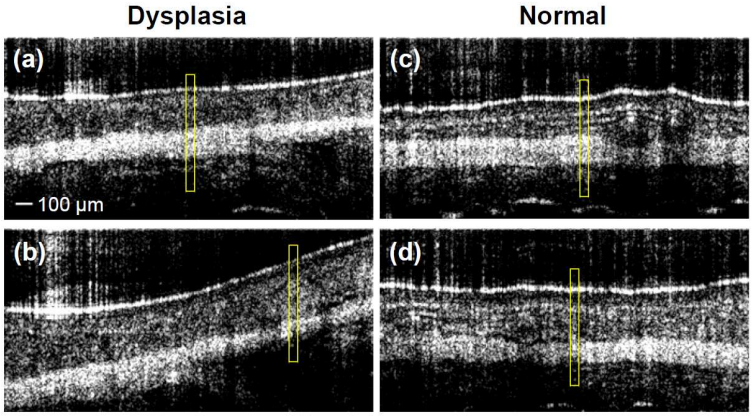

Fig. 6. SD-OCT images of *in vivo* oral dysplasia and normal tissues. (a) Dysplastic tissue before application of dMNs and US, (b) dysplastic tissue after both dMNs and US were applied, (c) normal tissue before dMNs and US were applied, (d) normal tissue after both dMNs and US were applied. Yellow areas were quantitatively analyzed for OCT signal intensity in Fig. 7.

#130172 - $15.00 USD Received 15 Jun 2010; accepted 7 Jul 2010; published 14 Jul 2010

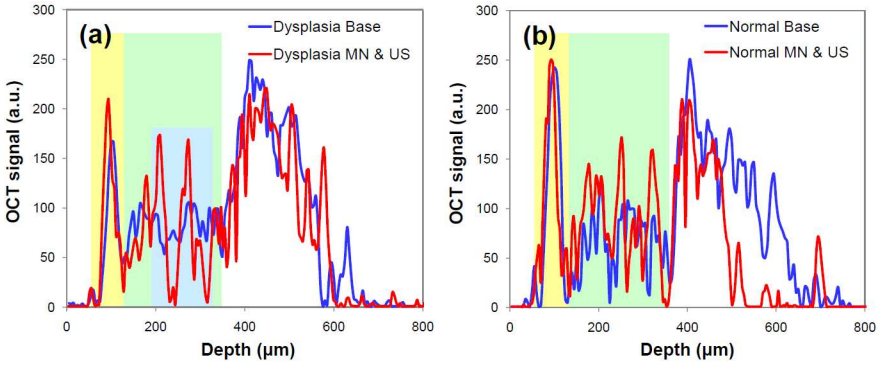

Fig. 7. Depth-dependent SD-OCT signal intensity profiles in dysplastic and normal hamster cheek pouch tissues. Yellow area: stratum corneum (SC); green area: epithelial layer; blue area: disrupted epithelial layer in dysplastic tissue.

The distinctive OCT images (Fig. 6) and signal intensity profiles (Fig. 7) in dysplasic and normal hamster cheek pouch tissues were compared with histological observations. As shown in Fig. 8, the epithelial layer in dysplastic tissue demonstrated disrupted stratification and epithelial thickening and downgrowth (yellow-dotted area). The appearance and morphology of the OCT image (Fig. 6b) and concurrent enhanced contrast of the deeper epithelial layers (Fig. 7a) paralleled the histological appearance of dysplasia (Fig. 8).

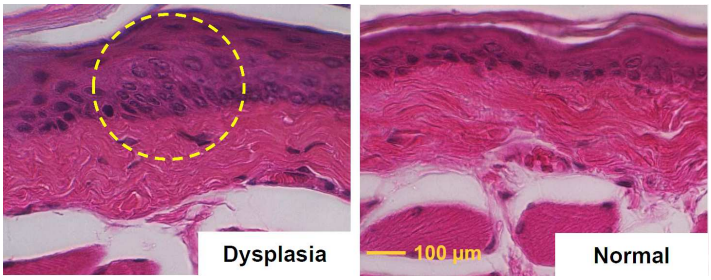

Fig. 8. H&E stained dysplastic and normal hamster cheek pouch tissues.

4. Conclusions

In order to enhance optical contrast for *in vivo* OCT imaging by overcoming structural barriers, such as the SC and mucosa, Au NPs were delivered in dMNs followed by a brief application of US. Considerably enhanced OCT images presenting clear structural differences between dysplastic and normal tissues were obtained. Quantitative analysis of OCT signal intensity profiles confirmed increased OCT signal intensity in the SC and dramatically increased optical contrast in dysplastic epithelium after Au NP-containing dMNs and US were applied. The interpretation of contrast-enhanced OCT images and signal analysis paralleled histological data. Penetration depth and Au NP doses can be easily tuned by adjusting the length of the dMNs and Au NP loading ratio, respectively. Therefore, dMNs are a promising and novel platform to deliver contrast agents across biological barriers in an efficient, convenient, precisely controlled, and potentially cost-effective manner.

Acknowledgement

We would like to thank Hongrui Li (Beckman Laser Institute) for her technical assistance with this study. This work was financially supported by the National Institute of Health (NIH) (3R21DE19298-02S1, EB-00293, EB-10090, RR-01192), AFOSR (FA9550-04-1-0101), the Beckman Laser Institute Endowment, the UC Cancer Center Support Grant (5P30CA062203-

13), and Council on Research Computing and Libraries Multi-Investigator Research Award (MI 23-2009-2010, UC Irvine).

#130172 - $15.00 USD Received 15 Jun 2010; accepted 7 Jul 2010; published 14 Jul 2010